suspected. In fact, particles behaving like Lambert spheres provide quite a good fit to the observed A- and B-ring brightness.

However, the C ring has noticeably different properties. For an optical depth ~0.1 (refs 15, 17), the C ring would be nearly as bright as the A and B rings at the present epoch, if the constituent particles were identical. However, Voyager observations show it to be less than half of the A and B brightness. Fuller phase-angle coverage, obtained subsequently in the mission, will be required for a distinction to be made between albedo and phase-function effects. However, the unambiguous implication is that the C-ring particles are different, either darker or more highly forward scattering than the A- and B-ring particles. This qualitative conclusion is consistent with the conclusions of recent analyses of Pioneer Saturn data[15,18]. This observation argues very strongly for a different particle population in the C ring as compared with the main rings. More data and analysis will refine these preliminary conclusions.

The figures and much of the data reduction for this article were provided by the Image Processing Laboratory at the Jet Propulsion Laboratory. We particularly thank G. W. Garneau and L. R. Doyle for assistance. G. E. Hunt is supported by the SRC. This report presents the results of one phase of research carried out at JPL under NASA contract NAS7-100.

Note added in proof: Subsequent Voyager observations have shown the azimuthal features which appear dark in back-scattered light reverse contrast and appear bright against the background B ring in forward-scattered illumination. This behaviour indicates that these features result from concentrations of small particles (a few micrometres) and not from variations in the B-ring particle density.

Received 31 October; accepted 17 November 1980.

1. Smith, B. A. *et al. Space Sci. Rev.* **21**, 103 (1977).
2. Danielson, G. E. *et al.* (in preparation).
3. Alexander, A. F. O'D. *The Planet Saturn* (Faber and Faber, London, 1962).
4. Cook, A. F. II, Franklin, F. A. & Palluconi, F. D. *Icarus* **18**, 317 (1973).
5. Kliore, A. J. *et al. J. geophys. Res.* (in the press).
6. Gehrels, T. *et al. Science* **207**, 434 (1980).
7. Dollfus, A. *Icarus* **12**, 101 (1970).
8. Ingersoll, A. P. *et al. Science* **207**, 439 (1980).
9. Reese, E. J. *Icarus* **15**, 466 (1971).
10. Franklin, F. A. & Columbo, G. *Icarus* **12**, 338 (1970).
11. Dollfus, A. *IAU Circ.* No. 1995 (1967).
12. Fountain, J. W. & Larson, S. M. *Icarus* **36**, 92 (1978).
13. Smith, B. A. *et al. Bull. Am. astr. Soc.* **12**, 727 (1980).
14. Kawata, Y. & Irvine, W. M. in *The Exploration of the Solar System* (eds Woszczyk & Iwaniszewska) (Reidel, Boston, 1974).
15. Esposito, L., Dilley, J. P. & Fountain, J. W. *J. geophys. Res.* (in the press).
16. Hansen, J. E. *Astrophys. J.* **155**, 565 (1969).
17. Cuzzi, J. N. in *The Saturn System* (eds Hunten, D. M. & Morrison, D.) (NASA CP-2068, 1978).
18. Gehrels, T. *J. geophys. Res.* (in the press).

Planform of mantle convection beneath the Pacific Ocean

Dan McKenzie*, Anthony Watts†, Barry Parsons‡ & Micheline Roufosse§

* Bullard Laboratories, Department of Earth Sciences, University of Cambridge, Madingley Road, Cambridge CB3 0EZ, UK
† Lamont-Doherty Geological Observatory and Department of Geological Sciences of Columbia University, Palisades, New York 10964
‡ Department of Earth & Planetary Sciences, MIT, Cambridge, Massachusetts 02139
§ Smithsonian Astrophysical Observatory, Cambridge, Massachusetts 02138

The correlation between variations of the bathymetry and of the geoid in the Pacific Ocean suggests that both are the surface expression of mantle convection. The planform of the convection which is required to generate the observed anomalies does not consist of rolls but is three dimensional, with rising and sinking jets elongated in the direction of motion of the Pacific plate relative to the frame of reference defined by the hot spots. The spacing between the maxima and minima of the geoid is between 1,500 and 2,000 km and hence favours a model of mantle convection with multiple scales of circulation.

ALTHOUGH most geophysicists agree that plate motions are maintained by mantle convection, there is little agreement about the geometry of the motion which converts heat into work. One of the principal difficulties is that the motion of the plates themselves provides a few restrictions on the form of the flow, because their motion can be described by rigid body rotations. Runcorn[1] recognized that long-wavelength gravity anomalies should be directly related to the fluid motion, and McKenzie *et al.*[2] showed that upper surface of the convecting region with constant viscosity was elevated, producing a positive gravity anomaly, over the rising region of the flow. The influence of the elastic forces within the plate on the magnitude and sign of the anomalies of gravity and bathymetry above a convecting region[3,4] is small if their wavelength is >500 km and the elastic thickness of the plates is ≤ 30 km (ref. 5). The wavelengths are expected to be at least twice the depth of the convecting region, or $>1{,}400$ km, if the convection is confined to the upper mantle. The amplitudes of the gravity and bathymetry anomalies obtained from the numerical calculations are about 20 mGal and 500 m respectively. Hence the anomalies should be easily observed, correlated with each other, and be little affected by the elastic behaviour of the plates. Two difficulties must be overcome before geophysical observations can be used to examine the convective planform. The first involves corrections to the observed bathymetry to remove the effects of lithospheric age, determined from the magnetic anomalies, and of sediment loading. Both of these can now be calculated with reasonable accuracy, and the depth obtained after these corrections has been applied is known as the residual depth. Only that part of the residual depth which is not produced by variations in crustal thickness and whose wavelength is longer than ~500 km is dynamically maintained by the convection. The other difficulty concerns the gravity field. Surface observations contain large amplitude short wavelength anomalies, and long wavelength errors are produced by drift of the instrument and calibration errors. For these reasons the long wavelength gravity anomalies can only be reliably obtained from surface ship observations in areas where there is dense coverage.

Historical techniques

The first attempt to use these arguments to investigate mantle convection[6] used the depth of the ridge axis and a satellite-derived gravity field. The procedure avoided the use of depth corrections, as the age of the ridge axis is the same everywhere and the sediment cover is very thin. Although the correlation between gravity and residual depth was clear in the North Atlantic, where it agreed with the numerical calculations, it was much less convincing in the other oceans. This behaviour was probably produced by errors in the satellite gravity field, whose

0028-0836/80/490442—05$01.00

higher harmonics were poorly determined. Extensive two-dimensional investigations of gravity and residual depth anomalies in the North Atlantic[4] and the Pacific around Hawaii[7] using surface gravity observations showed good agreement with the numerical models but neither covered a large enough area to demonstrate the convective planform. Cochran and Talwani[8] considered a larger region but failed to find a global relationship between gravity and residual depth similar to that found in the smaller regions[4,7]. Their lack of success was probably due to the poor sampling of the long-wavelength part of the gravity field due to the wide spacing of the ship tracks. Figure 3 shows that the amplitude of the gravity anomalies corresponding to 10 m variations in geoid height is only ~20 mGal. Such gravity anomalies will be difficult to detect in the presence of short wavelength anomalies of hundreds of mGal produced by seamounts, and measurement errors of at least 10 mGal. Menard and Dorman[9] attempted to use the bathymetry alone to examine the convective planform. Because long-wavelength variations in bathymetry may be isostatically compensated, and hence be unrelated to mantle convection, it is not obvious what constraints a study of the bathymetry alone imposes on the form of the circulation (see Fig. 2). An attempt[10] to obtain a gravity field over the Pacific from satellite orbits and surface gravity seems to have produced spurious anomalies, due to lack of sufficient surface observations and an instability caused by downward continuation[11].

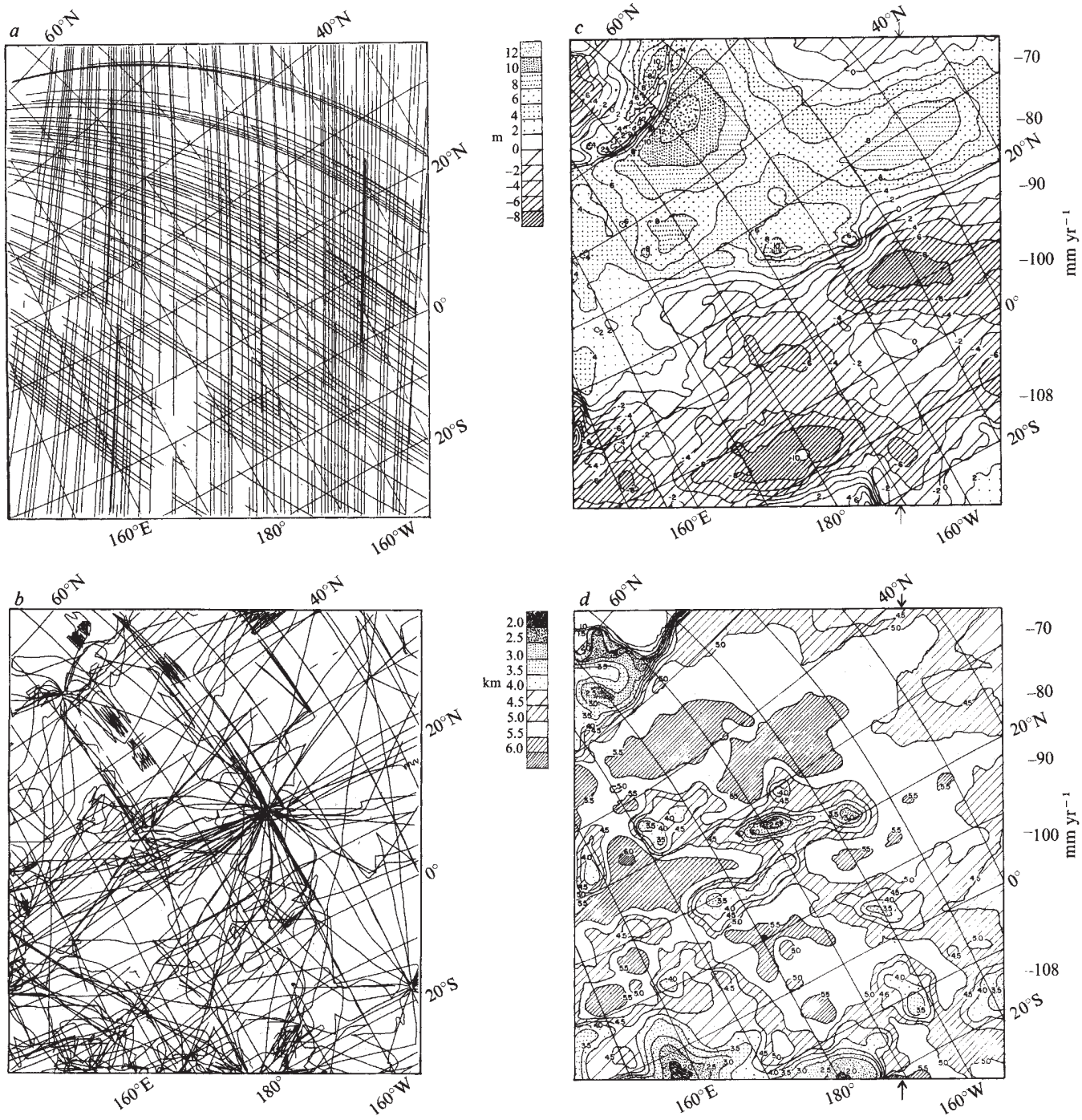

Fig. 1 Satellite altimeter (*a*) and ship (*b*) tracks used to obtain contour maps of geoid (*c*) and bathymetry (*d*) in the North and Central Pacific. The projection is an oblique mercator projection with axis 61.7°N, −82.8°E. Contour intervals are 2 m for (*c*) and 0.5 km for (*d*). The grid spacing in both cases is 100 km at the equator of the projection, and the gaussian half width for interpolation is 110 km for (*c*), 150 km for (*d*). The velocities shown on the right of (*c*) are those of the Pacific plate, moving from right to left, relative to the hot spot frame[15], and is 108 mm yr^{-1} at the equator of the projection.

A detailed analysis of the gravity field and surface deformation above different types of convection[12] showed that their ratio depends little on the form of the heating, the Rayleigh number, or the boundary conditions. Hence little further progress could be made until more accurate estimates of gravity anomalies between wavelengths of 500 km and 5,000 km became available over large areas of the oceans. GEOS 3 has now provided such estimates by direct determination of the geoid.

GEOS 3 measurements

The GEOS 3 satellite contains a radar altimeter which measures the distance from the satellite to the sea surface. If the orbit of the satellite and oceanographic corrections are known the geoid can be obtained directly. In practice, the precision of the altimeter is between 0.5 and 1 m, and analysis of the cross-over errors between different tracks shows errors of ~10 m (ref. 13) due to orbit errors. The orbit errors can be reduced to about 0.6 m by adjusting the orbits to minimize the cross-over errors[13]. We used these adjusted heights. Oceanographic corrections consist of tides and both time-dependent and steady-state variations produced by currents. These corrections are poorly known, but are probably <1 m in most parts of the ocean and were therefore ignored. The heights h_i corrected for bias and trend[13], at points described by radial unit vectors $\mathbf{a}_i$ were then filtered with a gaussian filter to give a smoothed height H_i at position $\mathbf{b}_i$

$$H_i = \sum_j h_j\omega_j \Big/ \sum_j \omega_j, \qquad \mathbf{b}_i = \sum_j \mathbf{a}_j\omega_j \Big/ \sum_j \omega_j$$

$$\omega_j = \exp(-d_j^2/\sigma^2) \tag{1}$$

where d_j is the distance between a chosen point on the profile and $\mathbf{a}_j$, and σ is the half width of the gaussian filter, chosen to be 100 km. In addition a weight W_i was obtained from the ratio of the rectangular approximation to the integral of the filter to the true integral

$$W_i = S\sum_j \omega_j/\sigma\sqrt{\pi}$$

where S is the spacing between successive points on the profile. If $W_i < 0.3$ the point was rejected. This processing reduced the number of data points while leaving unchanged longer wavelength features of the geoid. Because the geoid is dominated by long wavelength anomalies ($\lambda > 5{,}000$ km) and we are principally interested in those of intermediate wavelength, we subtracted the GEM7 geoid[14] up to and including $l = m = 10$. GEM7 was used because this geoid was determined from satellite orbits alone, and because the coefficients of degree and order <10 agree excellently with those of more recent determinations. The points $\mathbf{b}_i$ were projected onto a plane to give a position $\mathbf{x}_i$, and H_i then interpolated onto a square mesh using equation (1) with $\sigma = 110$ km, d_j being the distance between a mesh point and $\mathbf{x}_j$ in the plane of the projection, provided $d_j < 4\sigma$. Otherwise ω_j was set to zero. Finally the grid values were machine contoured. The bathymetry obtained from digitized profiles of more than 400 cruises in the Pacific Ocean treated similarly, except for the interpolation onto a square mesh where $\sigma = 150$ km was used.

Results

Figure 1 shows contour maps of the geoid and bathymetry, together with the satellite and ship tracks used. The area was chosen because it is large and well studied. Except in the upper right-hand corner of Fig. 1 sediment thicknesses are thin and uniform, and hence sediment loading corrections, which were not made, will produce little change in Fig. 1*d*. The depths in Fig. 1 have also not been corrected for subsidence as the lithosphere cools. Such corrections are also only important in the upper right-hand corner of Fig. 1, because the remainder of the area studied is underlain by lithosphere older than 60 Myr. The projection is an oblique mercator projection with the pole of relative motion between the Pacific plate and the hot spot frame as an axis[15], and the mesh spacing in Fig. 1*c*, *d* is 100 km on the equator of the projection. The region shown in Fig. 1 covers most of the North and Central Pacific. An accurate short wavelength anomaly produced by the Aleutian Island Arc is clearly visible at the top left of Fig. 1*c*, the anomaly on the left-hand edge is produced by the Mariana Island Arc, and those along the bottom by the Solomon and Tonga arcs. The geoid contours show the existence of elliptical maxima and minima whose amplitude is about 8 m and whose separation is between 1,500 and 2,000 km. One of the largest of these anomalies is associated with the Hawaiian Swell and has already been mapped using ship profiles[5]. The anomalies in Fig. 1*c* are too large and their separation is too great to be supported by the elastic part of the lithosphere, and therefore they must be dynamically maintained by mantle convection. Figure 1*d* shows that many of the geoid anomalies in Fig. 1*c* are associated with bathymetric anomalies. Figure 2 shows two profiles obtained from the values of the geoid and the bathymetry on the mesh points and plotted against distance in the oblique mercator projection to show the correlation more clearly. These two profiles are in the eastern part of the Pacific, where the geoid anomalies are large. The shoal region at the northern end of the profile is produced by the young lithosphere near the Gorda and Juan da Fuca ridge crests. This bathymetric anomaly does not correlate with the geoid and will be removed by the age corrections which have not yet been applied. Such corrections will not remove depth variations which are maintained by variations in crustal thickness, produced by vulcanism either on ridge axes or within plate interiors. Two such features, the Line Islands ridge and the Manihiki Plateau, are crossed by the profiles in Fig. 2 and both were produced by ridge axis vulcanism. Neither the crustal thickness nor the density of such ridges is well known, and therefore corrections are hard to apply. Towards the trench systems in the west the geoid is flatter than in the east, and several small anomalies of 2 and 4 m are associated with some of the large aseismic plateaus, such as the Shatsky and Hess Rises. Ridge axis vulcanism, which builds aseismic ridges at or above sea level on thin lithosphere, gives rise to anomalies of this magnitude, and there are many such features in the western Pacific[16].

The geoid anomalies in Fig. 1*c* are mostly elliptical, with the long axes of the ellipses approximately parallel to the x axis of the plot. As the projection is an oblique mercator projection whose axis is the pole of relative motion between the Pacific plate and hot spot frame, the rigid motion of the Pacific plate in Fig. 1*c* corresponds to a translation in the x direction. The relative velocity in this projection is $v_0 \operatorname{sech} y$, where v_0 is the equatorial velocity and y is the vertical coordinate of the mercator projection, and is shown on the right of Fig. 1*c*. The ellipticity suggests that the convective pattern is elongated in the direction of motion. The contours provide evidence that the elongation increases with increasing velocity.

Discussion

The above observations provide various constraints on models of mantle convection. Perhaps the most important is that the geoid strongly suggests the existence of mantle convection whose horizontal scale is considerably smaller than that of the plates themselves, and that the elongation of the anomalies in one direction results from the shearing of the circulation by plate motions. Such a model has previously been proposed on theoretical grounds[3,17]; where it was argued that the spacing between the rising and sinking regions should be similar to the depth of the convecting layer, and that the planform of the flow would probably consist of rolls aligned with their axes in the direction of motion, at least beneath rapidly moving plates such as the Pacific. This conclusion was qualified by Skilbeck and McKenzie[18] who used an approximate method to examine the stability of a model suggested by Richter and McKenzie[19], which possessed a low viscosity zone beneath the plates which decoupled the horizontal movement of the plates from that of the mantle below. The calculations suggested that even the Pacific

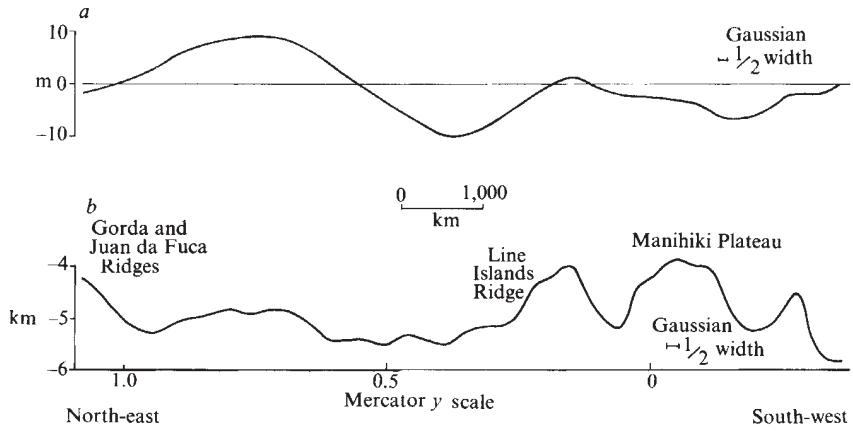

Fig. 2 Profiles of the geoid (*a*) and bathymetry (*b*) between the arrows on Fig. 1*c*, *d*. The horizontal axis shows the *y* coordinate in the oblique mercator projection, and the scale applies at $y = 0$.

was unlikely to be moving sufficiently fast to stabilize rolls, and that the small scale flow would probably be three dimensional. An alternative explanation is suggested by the experiments of Richter and Parsons[17] on the evolution of sheared convection. As the geometry of the Hawaiian Ridge requires the motion of the Pacific plate in the hot spot frame to have changed ~40 Myr ago, the present direction of motion may not have existed for long enough to have established rolls. It is obviously of interest to extend the observations of Richter and Parsons[17] to slower shearing rates.

Figure 3*a*, *b* and *c* shows the geoid, bathymetry and gravity produced by the convective flow in Fig. 3*d*, *e*. The depth of the convective layer is 700 km, the Rayleigh number is 1.4×10^6, and the flux is fixed at 58.5 mW m^{-2} on both boundaries (see refs 2 and 20 for details). Both horizontal and vertical scales are the same as those in Fig. 2 at the equator of the projection. Both the horizontal scale and the amplitude of the bathymetry and geoid in Fig. 3 are similar to those in the Pacific. Superimposed on the cellular circulation is a time-dependent flow driven by hot and cold blobs detaching from the boundaries. This flow produces obvious bathymetric and gravity anomalies, but the wavelength is too small to produce more than 1 m anomalies in the geoid. Similar numerical experiments with the more realistic boundary condition of a plate superimposed on top of the convecting region also show that the spacing is often considerably greater than the layer depth (G. Houseman, personal communication). Hence the geometry suggested by Fig. 1 is to be expected, and is not evidence for whole mantle convection.

An unexpected feature of the geometry of the geoid anomalies is that they are larger in the east where the plate is young than they are in the west where it is old. This distribution suggests that they are not the result of instabilities beneath the cooling plate, and hence are not related to the flow postulated by Parsons and McKenzie[21] to account for the observed relation between depth and age. The anomalies are better explained by instabilities of a lower hot boundary layer, perhaps at the base of the upper mantle. Near the trenches, where cold material is returned to the base of the convecting layer, the lower boundary layer is stable. As this material moves towards the east it is warmed by heat conducting into the upper mantle from the lower mantle, and becomes unstable. The same behaviour is clearly seen in the right-hand cell in Fig. 3*d*. The geoid anomalies are the surface expression of these instabilities.

Transfer of heat to the base of old lithosphere could still be produced by small cold blobs detaching from its base, similar to those on the right of Fig. 3*d*, because the geoid anomalies they would produce would be similar in magnitude to the noise (Fig. 3*a*). Such blobs would, however, produce obvious anomalies in the gravity field (Fig. 3*c*).

Some of the existing models of the return flow on a spherical Earth[22-24] show that the return flow is approximately antiparallel to the plate motion, and therefore can account for the elongation of the geoid anomalies in Fig. 1. All these models, however, neglect the thermal buoyancy forces in the interior of the convecting region. As such forces are dominant within large aspect ratio convective cells, such as that on the right in Fig. 3, the direction of flow obtained from the model calculations may not agree well with that in the mantle.

Conclusions

The observations discussed above have little relevance to whether the convective circulation involved in plate movements is confined to the upper mantle or extends throughout the whole mantle. If the whole mantle is convecting its Rayleigh number must be 10^9–10^{10} and the flow must be principally driven by internal heating. In these conditions the horizontal scale is

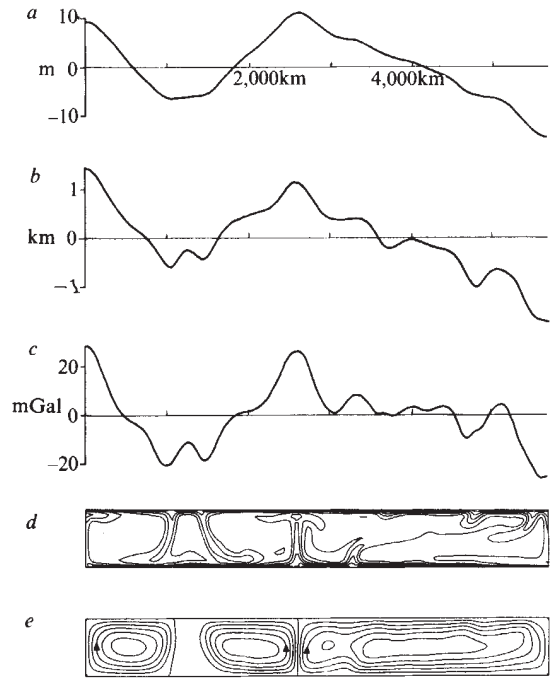

Fig. 3 Profiles of the geoid (*a*), bathymetry (*b*) and gravity (*c*) above a convecting fluid where the planform of the convection consists of two-dimensional rolls normal to the plane of the page. In all three cases the surface deformation obtained by the method outlined in ref. 12 has been convolved with the response of an elastic plate 30 km thick[3]. The horizontal scales are the same as those in Fig. 2 at the equator of the projection, and the vertical scales are the same. The temperature (*d*) contoured at 100°C intervals and the stream function (*e*) at 0.1 intervals are for a Rayleigh number of 1.4×10^6 with both upper and lower boundaries stress free and deformable. All the heat is supplied from below and the heat flux, not the temperature, is fixed on both boundaries (see ref. 20 for details).

controlled by the thickness of the boundary layer, and may be much smaller than the depth of the layer itself. In contrast, if the circulation is restricted to the upper mantle the boundary conditions[20] may produce a circulation whose horizontal scale is considerably greater than its depth (Fig. 3). Hence the horizontal scale is very little guide to the vertical extent of the flow. Nonetheless, the geometry of the anomalies is more easily explained by instabilities of hot lower boundary layer, which exists only if heat is supplied from below. Although the existence of such a boundary layer is required by models in which the flow is confined to the upper mantle, it is possible, though unlikely, that the unstable layer is as deep as the core–mantle boundary and that a considerable fraction of the heat is supplied from within the core. There is some evidence that models in which all the heat is supplied by internal heating are not compatible with the anomaly distribution, because instabilities can only originate in the upper boundary layer. The presence of large anomalies over the younger but not the older part of the Pacific suggests that the instabilities arise in the lower, not the upper, boundary layer.

We thank R. Rapp for providing the corrected altimetry profiles, and NASA, the Office of Naval Research, the NERC, and the Smithsonian Institution, for grants.

Received 13 June; accepted 19 September 1980.

1. Runcorn, S. K. *Phil. Trans. R. Soc.* A**258,** 228 (1965).
2. McKenzie, D. P., Roberts, J. M. & Weiss, N. O. *J. Fluid Mech.* **62,** 465 (1974).
3. McKenzie, D. P. & Weiss, N. O. *Geophys. J. R. astr. Soc.* **42,** 131 (1975).
4. Sclater, J. G., Lawver, L. A. & Parsons, B. *J. geophys. Res.* **80,** 1031 (1975).
5. Watts, A. B. *J. geophys. Res.* **83,** 5989 (1978).
6. Anderson, R. N., McKenzie, D. P. & Sclater, J. G. *Earth planet. Sci. Lett.* **18,** 391 (1973).
7. Watts, A. B. *J. geophys. Res.* **81,** 1533 (1976).
8. Cochran, J. R. & Talwani, M. *Geophys. J. R. astr. Soc.* **50,** 495 (1977).
9. Menard, H. W. & Dorman, L. M. *J. geophys. Res.* **82,** 5329 (1977).
10. Marsh, B. D. & Marsh, J. G. *J. geophys. Res.* **81,** 5267 (1976).
11. Watts, A. B. *J. geophys. Res.* **83,** 3551 (1978).
12. McKenzie, D. P. *Geophys. J. R. astr. Soc.* **48,** 211 (1977).
13. Rapp, R. H. *J. geophys. Res.* **84,** 3784 (1979).
14. Wagner, C., Lerch, F., Brownd, J. & Richardson, J. *J. geophys. Res.* **82,** 901 (1977).
15. Minster, J. B. & Jordan, T. H. *J. geophys. Res.* **83,** 5331 (1978).
16. Watts, A. B., Bodine, J. H. & Ribe, N. M. *Nature* **283,** 532 (1980).
17. Richter, F. M. & Parsons, B. *J. geophys. Res.* **80,** 2529 (1975).
18. Skilbeck, J. N. & McKenzie, D. P. *Pageophysics* **117,** 958 (1979).
19. Richter, F. & McKenzie, D. *J. Geophys.* **44,** 441 (1979).
20. Hewitt, J. M., McKenzie, D. P. & Weiss, N. O. *Earth planet. Sci. Lett.* **51** (in the press).
21. Parsons, B. & McKenzie, D. P. *J. geophys. Res.* **83,** 4485 (1978).
22. Parmentier, E. M. & Oliver, J. E. *Geophys. J. R. astr. Soc.* **57,** 1 (1979).
23. Chase, C. G. *Geophys. J. R. astr. Soc.* **56,** 1 (1979).
24. Hager, B. H. & O'Connell, R. J. *J. geophys. Res.* **84,** 1031 (1979).

Vesiculation of mafic magma during replenishment of silicic magma reservoirs

J. C. Eichelberger

Sandia National Laboratories, Albuquerque, New Mexico 87185

Mafic inclusions are lower in bulk density than the andesitic and dacitic lavas in which they occur, and apparently represent a foam inflated during rapid cooling of wet mafic magma in contact with cooler, more silicic reservoir magma. This process occurs as mafic magma enters the base of the reservoir, so that the mafic/silicic interface becomes unstable in Rayleigh–Taylor fashion. Mixing in these reservoirs thus depends on water content of mafic magma and pressure.

MAFIC inclusions in andesitic and dacitic lavas and in equivalent plutonic rocks have been interpreted as cumulates from fractional crystallization[1], restites from deep crustal melting[2] and rapidly crystallized mafic magmatic material generated during magma mixing[3]. The implications of these interpretations for both magmatic and crustal evolution differ dramatically. I have previously argued that the inclusions result from magma mixing on the basis of their texture, bulk composition and phase composition[4–6]. A new observation is that the inclusions exhibit high vesicularity and consequently have a lower bulk density than their hosts. This property is consistent with generation of the inclusions by magma mixing, and may play an important part in the evolution of large magma reservoirs within the upper crust.

Origin of mafic inclusions

Intermediate composition calc-alkaline volcanic and plutonic rocks commonly contain fine-grained mafic inclusions which appear as dark clots or blobs ranging from a few millimetres to a few tens of centimetres in diameter. Despite differing geological settings of the igneous complexes in which they occur, these inclusions display remarkably uniform textures, compositions and physical properties. In volcanic rocks the inclusions are dominantly plagioclase + hornblende + glass or plagioclase + pyroxene + glass. In plutonic rocks, a felsic matrix is present instead of glass and the dominant mafic phase if usually hornblende or biotite. Several observations indicate that the inclusions represent mafic magma injected into and chilled within cooler, more silicic magma reservoirs.

(1) Most inclusions are subspherical in shape, unlike accidental xenoliths derived from solid or nearly solid wall rock.

(2) In bulk composition and phenocryst content (typically calcic plagioclase and magnesian olivine) inclusions resemble associated mafic lava. This should not be the case for cumulates, the composition of which is controlled by the crystallizing magma and physical properties of the precipitating phases.

(3) Inclusions have an igneous texture characterized by abundant, elongated, strongly zoned, euhedral crystals in residual glass, indicative of rapid cooling and crystallization to just above solidus. This texture differs from the glassy or microcrystalline groundmass characteristic of mafic magma quenched at the surface. It also differs from the partial melt texture to be expected in restites.

(4) Some large inclusions exhibit outwards decrease in grain size, increase in elongation of grains, and/or an outer hybrid rind containing reacted or resorbed phenocrysts from the host lava. These observations indicate that the inclusions were chilled against the host, but that both host and inclusions were molten at the same time.

(5) Phenocrysts in the host lava are reacted or resorbed, consistent with heating of reservoir magma during cooling and crystallization of the inclusions.

These observations are further discussed elsewhere[4–6]. Important implications are that crustal magma reservoirs are

0028-0836/80/490446—05$01.00